Quasi-coherent chorus properties: 1. Implications for wave-particle interactions

Bruce T. Tsurutani,[1] Barbara J. Falkowski,[1,2] Olga P. Verkhoglyadova,[1,3] Jolene S. Pickett,[4] Ondrej Santolík,[5,6] and Gurbax S. Lakhina[7]

Received 26 October 2010; revised 13 June 2011; accepted 29 June 2011; published 10 September 2011.

[1] A study of dayside ELF/VLF electromagnetic (EM) waves from L* = 2 to 9 and magnetic local time (MLT) from 09 to 15 was conducted using plasma wave data from the Polar spacecraft. EM waves were detected from L* = 4 to 9 from 09 to 12 MLT with a decrease in the afternoon sector (12 to 15 MLT). Some of the chorus was clearly related to generation by substorm injected ~5 to 100 keV electrons drifting from the midnight sector to the local noon sector. However, dayside chorus also showed two solar wind ram pressure dependences: increased (above average) pressures and unusually low pressures. Possible chorus generation mechanisms are discussed. Chorus detected by Polar away from the magnetic equator generation region (~25° to 55° magnetic latitude) was substantially different than chorus detected in previous studies within the ~0° to 10° generation region. (1) Two separate bands of chorus were often detected simultaneously: a higher-frequency downgoing (toward the Earth) band of waves and a lower-frequency upcoming band. (2) The downgoing waves are ~2 orders of magnitude more intense (~10^{-2} nT^2) than simultaneously detected lower-frequency upcoming waves (~10^{-4} nT^2). (3) Chorus, when viewed as a Fourier spectrum, appears as a band of semicoherent hiss. (4) A scenario and schematic is presented to explain these observations: chorus is presumed to be generated at the equator at large L*, propagate downward toward Earth and inward across L* shells, and then refract back up to the spacecraft location. (5) The waves detected at Polar latitudes did not possess the temporal structure or the coherency of the ~10 to 100 ms duration equatorial chorus subelements, although full single cycles with right-hand, circularly polarized structures were identified. This quasi-coherent EM turbulence may be formed by wave dispersive effects. The longer the wave path length, the greater is the reduction in coherency. (6) This feature of chorus has significant consequences for off-equatorial wave-particle interactions. For example, the microburst mechanism of Lakhina et al. (2010) that can account for rapid pitch angle diffusion of ~5 to 100 keV electrons in the chorus generation region will not work for off-equatorial scattering of relativistic electrons because of the lack of chorus coherence there. (7) Some comments about semicoherent chorus (hiss) in the outer magnetosphere are made as challenges to theorists in the field.

Citation: Tsurutani, B. T., B. J. Falkowski, O. P. Verkhoglyadova, J. S. Pickett, O. Santolík, and G. S. Lakhina (2011), Quasi-coherent chorus properties: 1. Implications for wave-particle interactions, *J. Geophys. Res.*, *116*, A09210, doi:10.1029/2010JA016237.

[1]Jet Propulsion Laboratory, California Institute of Technology, Pasadena, California, USA.
[2]Physics and Astronomy Departments, Glendale Community City College, Glendale, California, USA.
[3]CSPAR, University of Alabama in Huntsville, Huntsville, Alabama, USA.
[4]Department of Physics and Astronomy, University of Iowa, Iowa City, Iowa, USA.
[5]Institute of Atmospheric Physics, Prague, Czech Republic.
[6]Faculty of Mathematics and Physics, Charles University, Prague, Czech Republic.
[7]Indian Institute of Geomagnetism, Navi Mumbai, India.

0148-0227/11/2010JA016237

1. Introduction

[2] Chorus [*Gurnett and O'Brien*, 1964; *Burtis and Helliwell*, 1969] is the dominant electromagnetic wave detected in the Earth's outer zone radiation belt [*Tsurutani and Smith*, 1974, 1977; *Burton and Holzer*, 1974; *Burtis and Helliwell*, 1976; *Anderson and Maeda*, 1977; *Cornilleau-Wehrlin et al.*, 1978; *Koons and Roeder*, 1990; *Helliwell*, 1995; *Meredith et al.*, 2001, 2003; *Haque et al.*, 2010]. The waves are generated by an electron instability associated with anisotropic ~5–100 keV electrons [*Kennel and Petschek*, 1966; *Tsurutani and Smith*, 1974; *Tsurutani et al.*, 1979; *Tsurutani and Lakhina*, 1997; *Santolík et al.*,

2010a; *Schriver et al.*, 2010]. Chorus, through cyclotron resonance with the electrons, is believed to cause pitch angle scattering of energetic electrons into the loss cone [*Inan et al.*, 1978, 1992; *Inan*, 1987; *Summers et al.*, 2007a, 2007b; *Thorne et al.*, 2005; *Tsurutani et al.*, 2009; *Lakhina et al.*, 2010; *Hikishima et al.*, 2010] and create bremsstrahlung X-ray "microbursts" in the upper atmosphere at 80 to 100 km altitude [*Anderson and Milton*, 1964; *Parks*, 1967; *Parks and Winckler*, 1969; *Tsurutani*, 1972; *Nakamura et al.*, 2000; *Lorentzen et al.*, 2001a, 2001b]. Wave-particle interaction with chorus is also believed to be the main mechanism for the acceleration of ~100 keV electrons to relativistic energies, a major topic in space weather physics today [*Horne and Thorne*, 1998; *Summers et al.*, 1998, 2004; *Roth et al.*, 1999; *Albert*, 2002; *Meredith et al.*, 2002, 2003; *Horne et al.*, 2003a, 2003b, 2005a, 2005b; *Omura and Summers*, 2006; *Omura et al.*, 2007].

[3] Although chorus and other extremely low frequency (ELF) and very low frequency (VLF) electromagnetic (EM) waves have been studied using spacecraft measurements for decades, there are still regions in the magnetosphere where the properties of these waves are not well understood. One of the regions is the dayside outer zone. Chorus properties at magnetic latitudes away from the equatorial generation region have also not been studied in great detail. It is the purpose of this paper to use Polar plasma wave data to study the properties of chorus ELF/VLF EM waves from 09 to 15 MLT and from L* [*Roederer*, 1970] = 2 to 9. From a case study of a selection of high time resolution waveform data, we investigate the nature of the waves such as their amplitudes, polarization and coherency. This paper will be called paper I. This study will be followed by a second paper (paper II) that gives ELF/VLF EM wave statistical results. The main intent of both of these works is to provide EM wave properties that should be useful for wave-particle interaction modelers.

2. Data Analyses

[4] We performed a detailed examination of ELF/VLF EM waves in the dayside magnetosphere, with the primary focus on chorus. There are ~1.5 years where the Polar spacecraft Plasma Wave Instrument (PWI) [*Gurnett et al.*, 1995] was operational: 1 April 1996 to 16 September 1997. Selected portions of the available data were used in this study.

[5] The PWI 2 kHz high-frequency waveform receiver (HFWR) data [*Gurnett et al.*, 1995] that were recorded onboard the spacecraft were used in this study. The wave properties studied are: the wave Poynting vector relative to the ambient magnetic field direction, B_0, and the wave intensity, ellipticity, and planarity. The data are sampled in snapshots: 2048 samples simultaneously from each of six channels (three each orthogonal magnetic and electric antennas) over ~0.459 s time intervals (hereafter referred to as ~0.5 s intervals) with a time resolution of ~224 μs in the frequency range from ~20 Hz to ~2 kHz. The snapshots are obtained every ~128.8 s, thus creating a duty cycle of 0.459 s of data followed by a data gap of 128.34 s. For shorthand, hereafter the 128.8 s intervals are referred to as ~2 min intervals.

[6] Details of chorus properties obtained using Polar PWI data were previously reported by *LeDocq et al.* [1998], *Sigsbee et al.* [2008, 2010] and *Santolík et al.* [2010b]. The present study provides new insights into those chorus properties as it exclusively uses data from the 2 kHz mode of the PWI HFWR, unlike the previous works which used data from other PWI receivers and HFWR modes. The value of the data from the 2 kHz mode of the HFWR for studying chorus lies primarily in two areas: (1) the data are received on almost every orbit providing a better sampling of data for surveys and statistical studies and (2) the data are received with high time and frequency resolution from six channels, as discussed above, in a frequency band well matched to the chorus frequency range in the dayside outer zone. These data thus allow analyses of single wave cycle events giving polarization, direction of propagation and ellipticity information.

[7] A sample orbit of the Polar spacecraft is shown in Figure 1. This orbit occurred from ~15:50 UT 14 August to ~09:20 UT 15 August 1996. The top panel gives the orbit projected into the X-Z plane of the Geocentric Solar Magnetospheric (GSM) coordinate system. The bottom panel is the projection into the GSM X-Y plane. The EM wave detection interval for this orbit (discussed later with Figure 2) is shown in red. The satellite orbit is superposed on the Tsyganenko 04 [*Tsyganenko*, 2002] geomagnetic field model.

[8] Previous works have noted that chorus is primarily generated at the magnetic equator and in dayside minimum B pockets [*Tsurutani and Smith*, 1974, 1977; *Anderson and Maeda*, 1977; *LeDocq et al.*, 1998; *Meredith et al.*, 2001, 2003; *Lauben et al.*, 2002; *Horne et al.* 2005b; *Omura et al.*, 2008; *Verkhoglyadova and Tsurutani*, 2009; *Tsurutani et al.*, 2009] in the outer region of the magnetosphere. Polar generally does not enter these generation regions (except during magnetic storms), but does cross magnetic field lines that connect to them. Since chorus is an electromagnetic wave that can propagate both along and across the magnetic field lines, waves can propagate from their generation regions to Polar altitudes.

[9] Our study focuses on the dayside region of the magnetosphere. We have used L* and magnetic local time (MLT) to bin the data to do a study of chorus in this region. The L* parameter is used here because drifting energetic electrons, which generate chorus, should be ordered by L*. MLT was calculated based on magnetic dipole coordinates. The McIlwain L parameter [*McIlwain*, 1961] represents the radial distance in R_e (Earth radius) where a dipole magnetic field line intersects the geomagnetic equatorial plane. The L* parameter [*Roederer*, 1970] which we use here for the spacecraft position corresponding to all waveform snapshots, is the McIlwain L parameter modified for solar wind pressure and interplanetary conditions. To identify the L* value at any time, the ONERA-DESP library version 4.2 is used to determine the magnetic flux encompassed by a guiding drift shell of trapped 90° pitch angle particles. This L* determination uses the T89c model [*Tsyganenko*, 1989] for the external component of the magnetic field (based on Kp indices). Trapped 90° pitch angle particles, gradient drifting on a particular L* shell, will be closer to Earth at 12 MLT and farther from Earth at 24 MLT than the corresponding L value. We use a bin scale size of $\Delta L^* = 1$ and $\Delta MLT = 1$ for our unit area of resolution. We analyze these parameters from L* = 2 to 9. For a ELF/VLF wave "event," we use a sample interval of ~0.5 s, the intrinsic rate of the HFWR 2 kHz mode used in this study.

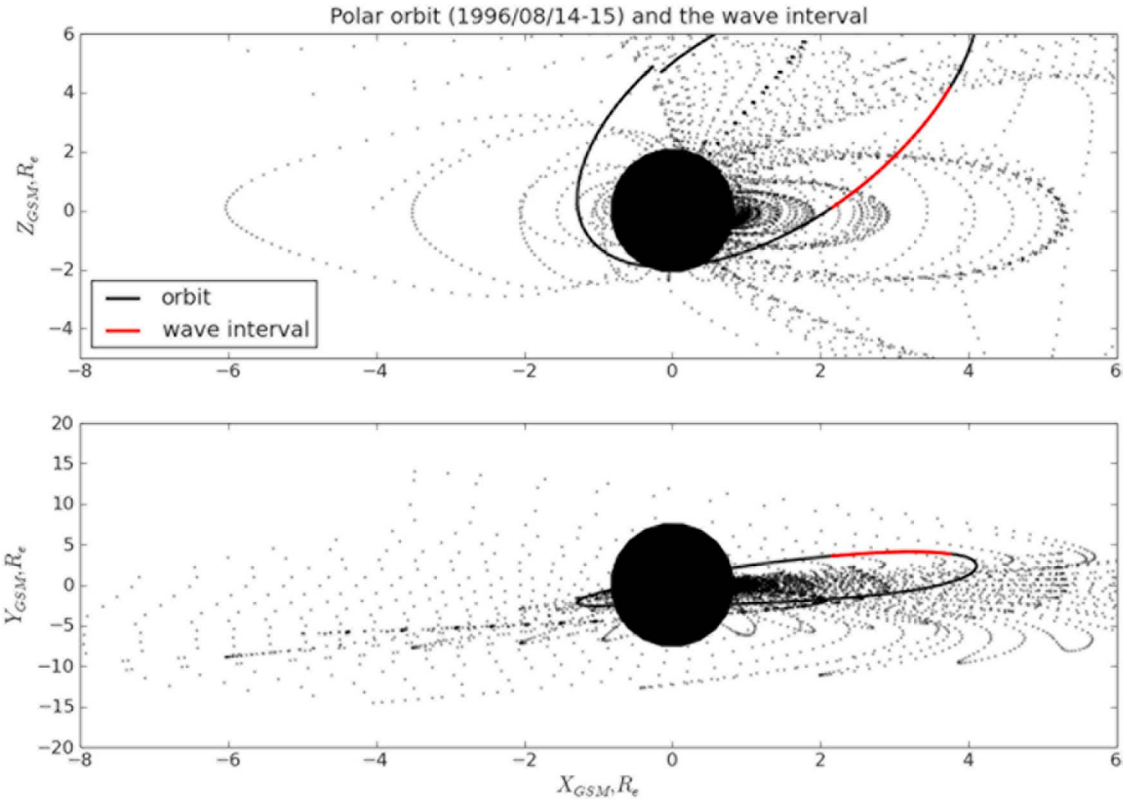

Figure 1. The Polar orbit from ~15:50 UT on 14 August 1996 to ~09:20 UT on 15 August 1996. The Tsyganenko T04 model and the OMNI solar wind data were used to construct the magnetic field lines in GSM coordinates. The field configuration was calculated at 03:00 UT on 15 August 1996 and projected into the X-Z and X-Y planes. The Sun is to the right. The electromagnetic (EM) wave interval is indicated in red. Chorus waves were detected from 03:00 to 05:10 UT (shown in red).

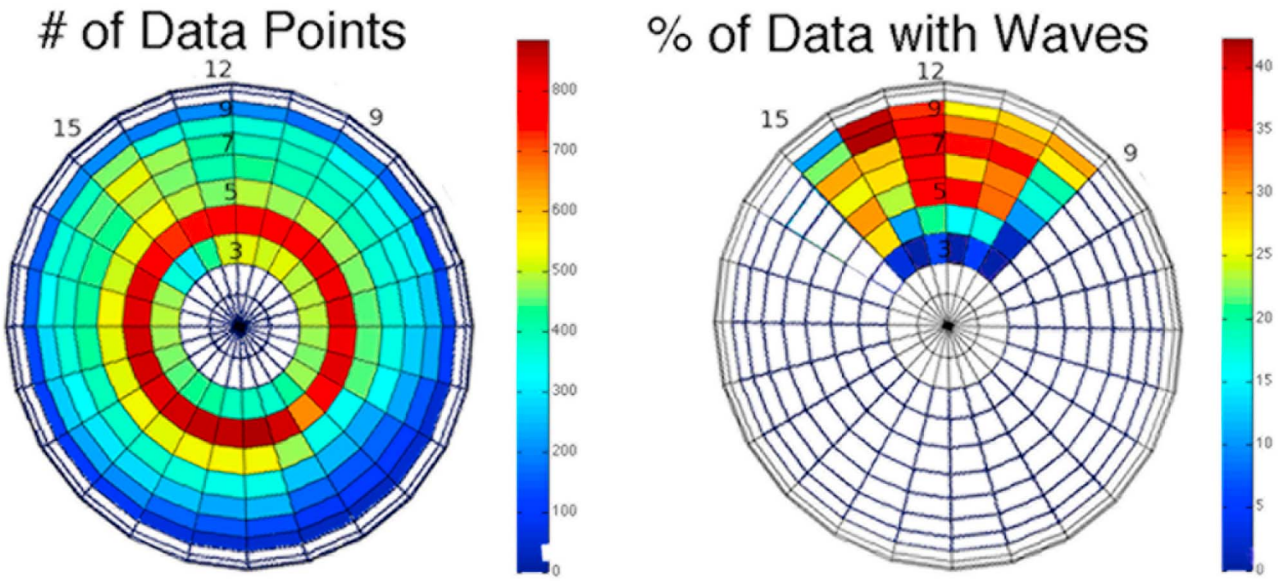

Figure 2. (left) The coverage of Polar for this study. Each potential wave "event" was defined as a ~2 min interval from L* = 2 to L* = 9 (the value of the constant L* curve is indicated below the line). The color coding indicates the number of "events" for each ΔL* = 1 and ΔMLT = 1 box with the scale given on the right. (right) The percent of the times that chorus is detected during the local time of interest, 09:00–15:00 MLT. The scaling of the latter is given on the right side.

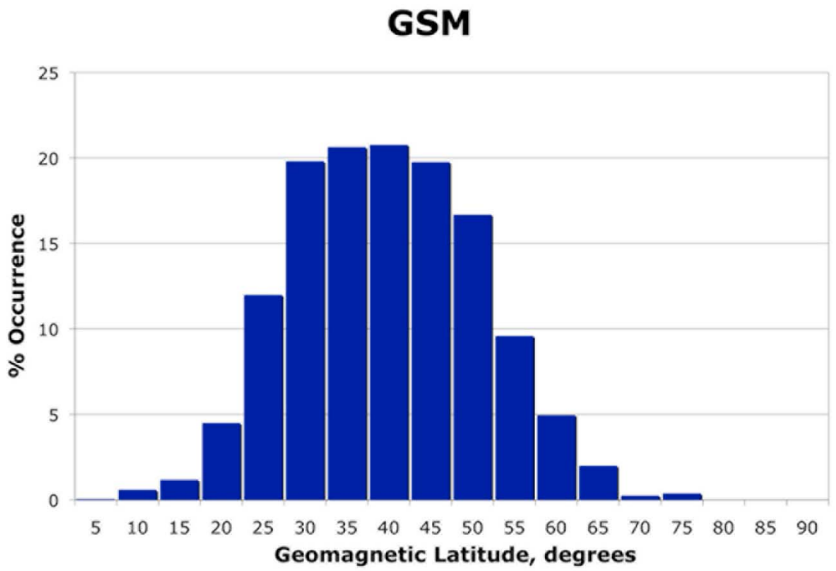

Figure 3. The latitudes where EM waves were detected in this study. The coordinate system is GSM. Note that the waves were detected primarily in middle latitudes and not near the equator (±10°) where the waves are believed to be generated.

[10] The solar wind and geomagnetic activity conditions are important external influences that affect the growth or lack of growth of chorus. Thus the analyses will begin with the chorus dependence on solar wind ram pressure, *AE* and *Dst*.

3. Results

[11] The left-hand panel of Figure 2 shows our spatial coverage for the Polar EM wave study. The L* value is listed below each line. The MLT 9, 12 and 15 h are given outside the circles. The MLT coverage is reasonably uniform with all times covered roughly equally. The L* coverage is maximum from L* = 3 to 4, with other regions covered more or less equally. Since the same local time intervals are covered twice each 6 months, the ~1.5 year interval of data represents ~6 passes through the MLT 9 to 15 dayside region of interest.

[12] Each wave interval was first identified by hand using the 2 kHz bandwidth HFWR summary data plots. The background for the wave plots was 10^{-9} nT^2Hz^{-1} for the BSUM (sum of the three spectral densities from the magnetic sensors) and 10^{-7} $mV^2m^{-2}Hz^{-1}$ for the ESUM (sum of the three spectral power densities from the electric sensors). Electrostatic waves (waves detected only in ESUM) were excluded from the study. General frequency increases were sought for waves detected as the spacecraft was inbound (to higher ambient magnetic field strengths) or frequency decreases when the spacecraft was outbound. Since chorus is generated at a fraction (~0.25 to ~0.75) of the electron cyclotron frequency [*Tsurutani and Smith*, 1974], over a wide range of L*, the general chorus frequency band increases when the spacecraft is traveling inbound (toward higher magnetic field strengths). Both the BSUM and ESUM spectral power densities were used to identify chorus wave intervals with these characteristics. When such long-term (~tens of minutes) rising/falling frequency bands were identified, nearby waves were also included in the study. The waves were next binned by L* and MLT into the intervals identified above by computer. Those wave events falling outside the MLT and L* constraints of the study, as described above, were discarded. This was the selection criterion used for chorus selection. We however cannot guarantee that some contamination by other EM mode waves may be present (as is true for all chorus statistical studies).

[13] The right-hand panel of Figure 2 shows the distribution of ELF/VLF waves identified in this study. What is shown is the percent occurrence for each L*-MLT bin. This is the number of times that ELF/VLF waves were detected divided by the total number of times that Polar passed through that particular bin times 100.

[14] Two interesting features are present in Figure 2. There is an asymmetry between chorus in prenoon and postnoon local times, with greater occurrence in the prenoon sector. There is a general lack of waves at very low L* values, inside L* = 4.

[15] Figure 3 gives the magnetic latitude distribution of the EM wave events. These are given in GSM coordinates. The distribution shows that most EM waves were detected at midlatitudes between ~25° and ~55°, with a median near ~40°. Few if any waves were detected inside ±10° of the equator, primarily because of orbital constraints (see Figure 1).

3.1. Background Conditions: Geomagnetic Activity and Solar Wind Ram Pressure

3.1.1. *Dst* Indices for EM Wave Interval

[16] Figure 4 gives the *Dst* (disturbance–storm time) index distribution for the ~1.5 years of Polar plasma wave coverage and also for the ELF wave events in Figure 2. The *Dst* for the entire interval is denoted in gray with the scale on the left. The mean value for the distribution is $Dst = -12.1$ nT. The *Dst* for the wave events is given in black with the scale on the right. The mean of the latter distribution is $Dst = -9.8$ nT. For comparative purposes, the mean *Dst* during March 2000 (solar maximum), was $Dst = -19.0$ nT, considerably more

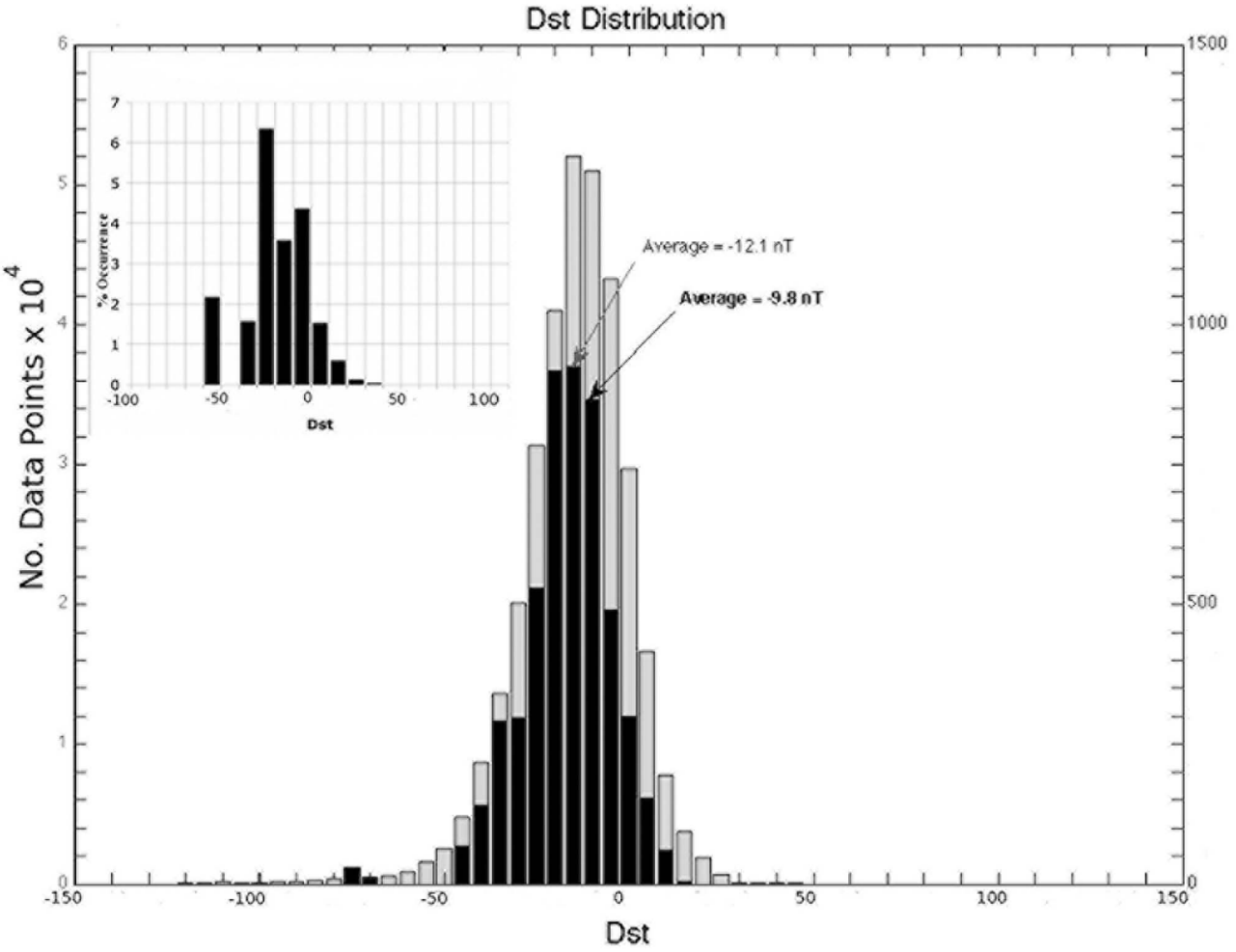

Figure 4. A distribution of the *Dst* values for the intervals of Figure 2. The total ~1.5 year Polar interval is given in gray, and the dayside chorus detection intervals are given in black. The scales for the total interval and the chorus intervals are given on the left and right, respectively. The normalized chorus interval is given as an insert.

negative than during this solar minimum (1996) interval study.

[17] The normalized *Dst* (the number of EM wave intervals divided by the total number of *Dst* events for that bin) is given in the insert at the upper left of Figure 4. The majority of the ELF events were detected when *Dst* was in the range of -40 nT < *Dst* < +20 nT with far more events occurring (percentagewise) when *Dst* was negative. Negative *Dst* values imply weak magnetic storm occurrences and positive *Dst* values indicate storm initial phases or enhanced solar wind ram pressure intervals [*Tsurutani et al.*, 1988, 2006; *Gonzalez et al.*, 1994]. Chorus waves detected during the solar cycle declining phase or during solar minimum are usually associated with high-intensity long-duration continuous *AE* activity (HILDCAA) injection events/substorms [*Tsurutani and Gonzalez*, 1987].

[18] The Polar data interval used here was collected during the minimum between solar cycles 22 and 23. There were only a few large *Dst* ≤ −100 nT storms during the 1996–1997 period. *Tsurutani et al.* [2006] have shown that there are ~15 to 20 times as many large magnetic storms at solar maximum than during solar minimum. The distribution of *Dst* in Figure 4 is what one might expect during solar minimum, a quiet period in terms of magnetic storm occurrence. With a lack of large magnetospheric storm time electric fields [*Gonzalez et al.*, 1994; *Tsurutani et al.*, 2006] to drive plasma sheet electrons deep into the magnetosphere, one would expect a general lack of chorus generation in the region at L* = 2 to 4. Figure 2 shows a lack of chorus occurrence frequency in this L* range, as expected.

3.1.2. *AE* Distributions

[19] Figure 5 gives the auroral electrojet (*AE*) index distributions for the ~1.5 years when Polar HFWR wave data were available. The Polar HFWR intervals and EM wave intervals are given in gray tone and in black, respectively. The scales are again on the left and right, respectively. To analyze the EM wave *AE* dependence, a time-shift for gradient drift of energetic electrons to the local time of observation was taken into account. An energy of ~20 keV (90° pitch angle) and a dipolar magnetic field were assumed [*Tsurutani and Smith*, 1977].

[20] The average *AE* for the whole interval is 169 nT and for the chorus intervals, 176 nT. The normalized *AE* distribution is given in the insert in the upper right. There is a slight

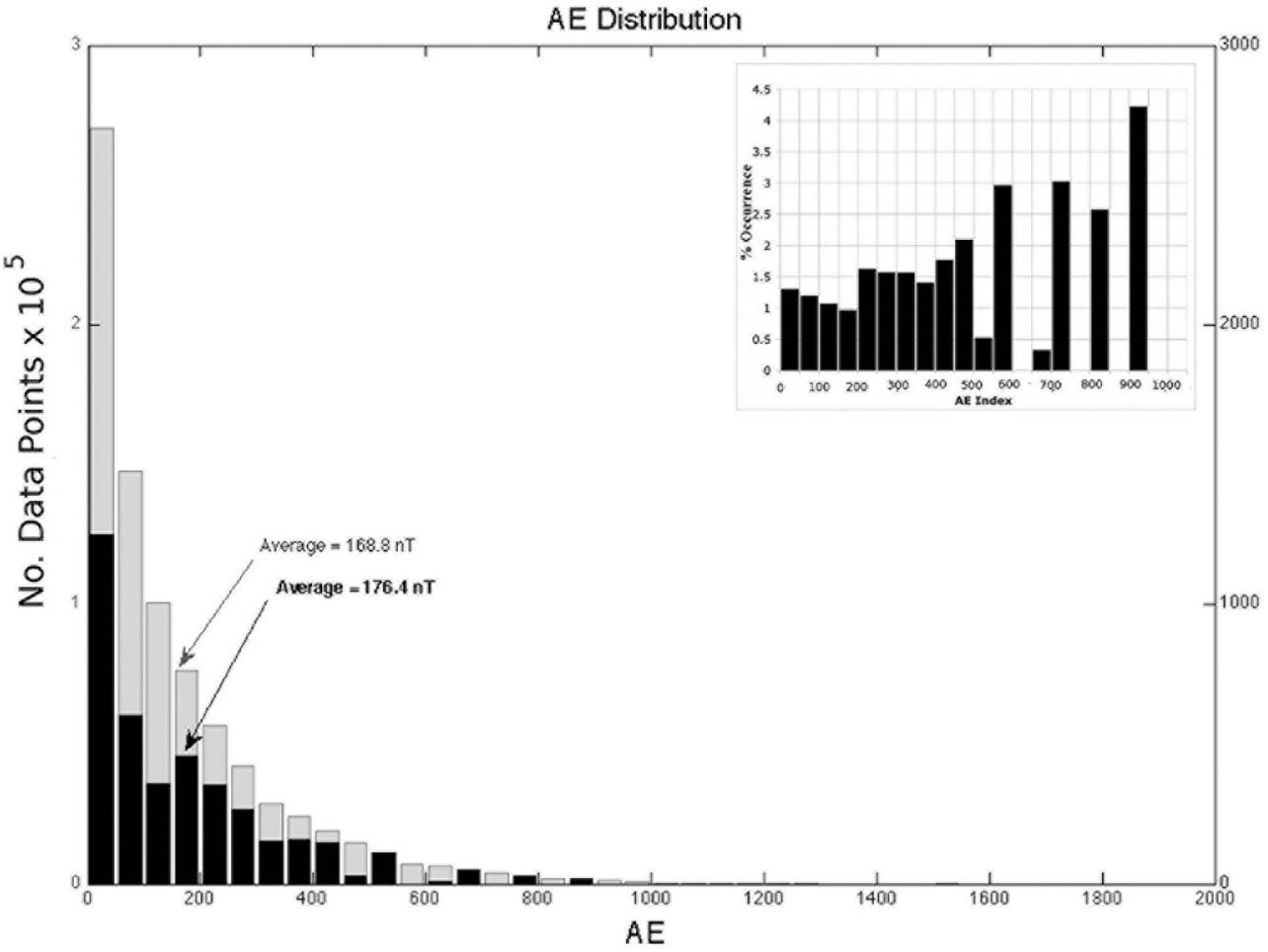

Figure 5. Same format as in Figure 4 but for the *AE* indices. The *AE* distribution for the whole Polar interval is indicated in gray and for chorus intervals in black. The insert gives the normalized chorus dependence on *AE*. It is noted that there are very few 2 min intervals where *AE* was >1000 nT. For most of the intervals *AE* was <100 nT. This is unusually quiet and corresponds to solar minimum conditions.

indication that the EM waves occur during higher *AE* values, consistent with the averages stated above. However, it is noted that there were *AE* intervals ranging from 1000 to 1600 nT (see main panel, Figure 5) where the EM waves were not present. This latter result does not imply a lack of correlation between chorus and high *AE*. Polar could have been outside of the selected L* or LT range during these times.

3.1.3. Solar Wind Ram Pressure

[21] The solar wind ram pressure influence on chorus generation was also examined. The solar wind propagation delays from ACE to the magnetosphere were removed. No other time shifts were assumed. Figure 6 shows the solar wind ram pressure during the Polar study. The data for the whole Polar interval is shown in gray and the scale is on the left. The mean pressure is ~2.4 nPa. The data with EM waves are shown in black with the scale on the right. The mean pressure is ~2.4 nPa, essentially the same value as the overall average of pressure during the Polar study. Both of these values were lower than a solar maximum value of ~2.9 nPa (March, 2000).

[22] The normalized pressure distribution is shown as an insert in the upper right. What is interesting is that the solar wind pressure during the EM wave events had a bimodal distribution. Waves are present when the solar wind pressure is less than 0.5 nPa and also when the pressure is 5 to 10 nPa.

3.2. Chorus Event Study: Properties of Downgoing and Upcoming Waves

[23] A Polar pass with chorus is given in Figure 7. We use the same analysis methods as used by *Santolík et al.* [2010b]. The top two panels indicate the presence of chorus by the sum of three magnetic components and three electric components, respectively. Chorus is the enhanced signals at ~100 Hz (02:50 UT) to >1 kHz (04:30 UT) as POLAR comes Earthward into higher magnetic field strengths. The threshold for detection/cutoff was discussed previously. The next two panels give the Poynting flux spectral density and the electron plasma frequency, respectively. The electron plasma frequency is useful to give the location of the high-density plasmasphere, from ~05:10 to ~06:10 UT. In this case the chorus waves are detected outside the plasmasphere (before ~05:10 UT). The next panel shows the angle θ of the direction of the Poynting vector of the wave relative to the magnetic field B_0. These data were taken in the northern hemisphere.

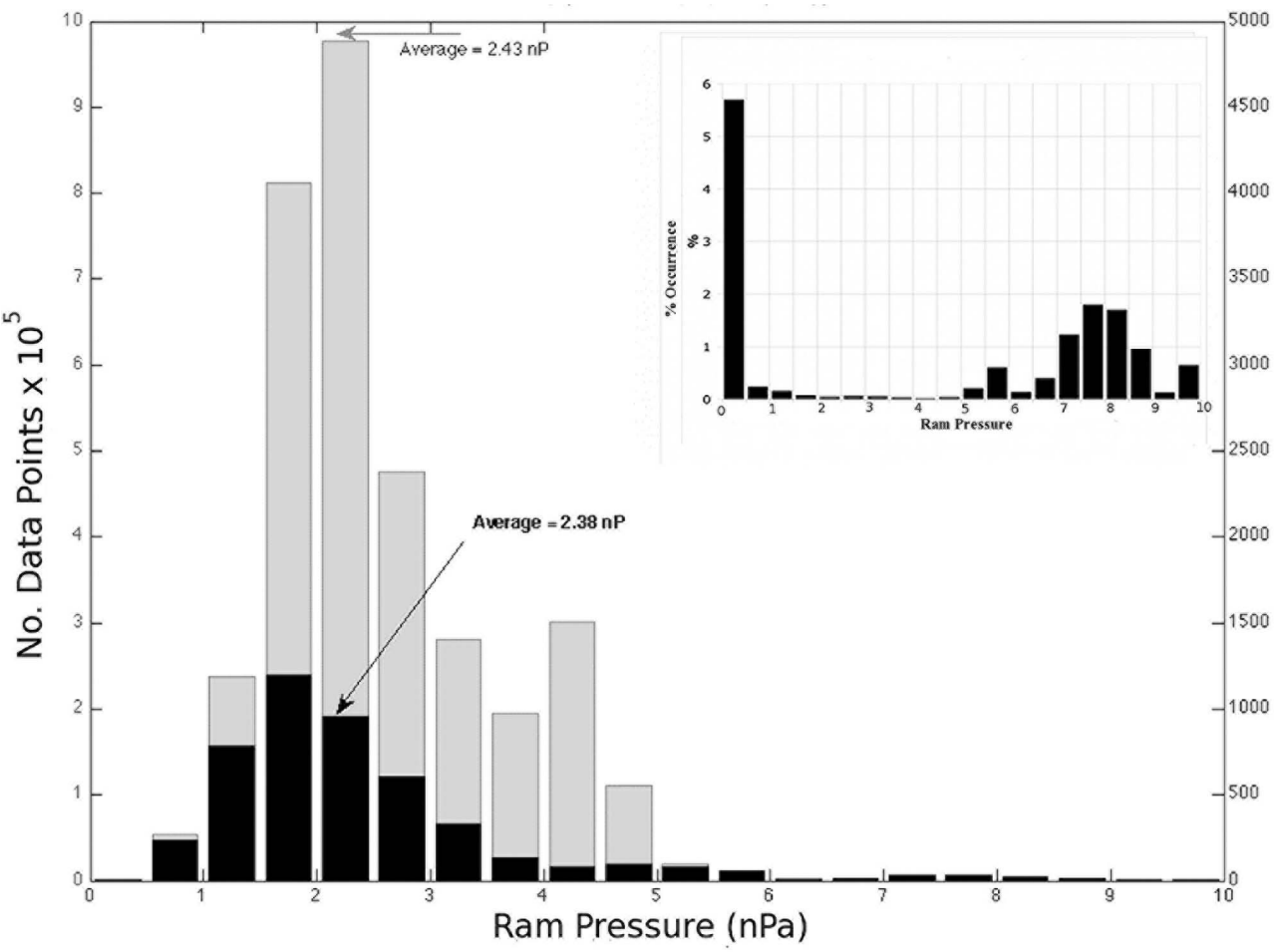

Figure 6. Solar wind ram pressure distributions for the Polar interval of study (gray tone with scale on the left) and also for the chorus events (black with scale on the right). The insert gives normalized chorus as a function of ram pressure. The normalized distribution has two dominant peaks: one at low pressures and a second at high pressures.

Here one can note that there are two main wave directions, one in the direction along the ambient magnetic field (blue) toward the Earth and one in a direction opposite the magnetic field (red) away from the Earth. The downgoing waves and upcoming waves are present at the same time, with the downgoing waves having a frequency higher than the upcoming waves. It can be noted by comparing the top three panels, that the downgoing (blue) waves were more intense than the upcoming (red) waves. We return to these points later. The last panel gives the wave ellipticity of polarization. The waves are noted to be right-hand polarized, consistent with whistler mode chorus emissions.

[24] The presence of downgoing higher-frequency waves with simultaneous upcoming lower-frequency waves was a typical feature found in this Polar plasma wave study [see also *Santolík et al.*, 2010b]. We illustrate this one particular case to investigate the detailed nature of both waves detected in the outer magnetosphere.

[25] Figure 8 contains the results of an analysis of a ~0.5 s interval of downward propagating waves at ~03:20:50 UT in Figure 7. Figure 8a shows the local wavelet power spectrum of one magnetic component of the waves perpendicular to B_0 for one frame of data (2048 samples = 459 ms). A continuous wavelet transform using the Morlet mother wavelet function was chosen to analyze these data. The Morlet wavelet, which consists of a plane wave modulated by a Gaussian, was chosen because it has zero mean, is localized in both time and frequency space, has several smooth oscillations and its period (inverse frequency) is a well-defined quantity that approximates the period of a signal obtained through Fourier analysis. The wavelet transform analysis was chosen because the data time series is nonstationary, i.e., although it exhibits a dominant range of frequencies, these frequencies and their amplitudes change quite rapidly. We are interested in wave power changes with time, so have used this technique for the display. The reader is referred to *Torrence and Compo* [1998] for more information on the use of wavelet analyses in geophysics.

[26] Figure 8a shows that most of the power of the waves is concentrated in the frequency range ~100–500 Hz. This corresponds to the downgoing (blue) waves shown in Figure 7. There is structure in the waves, but not the nice rising or falling tones of chorus elements detected close to the equator/generation region. The Fourier spectrum of the same magnetic component is shown in Figure 8c. From this perspective this chorus is similar to "hiss," although the waves

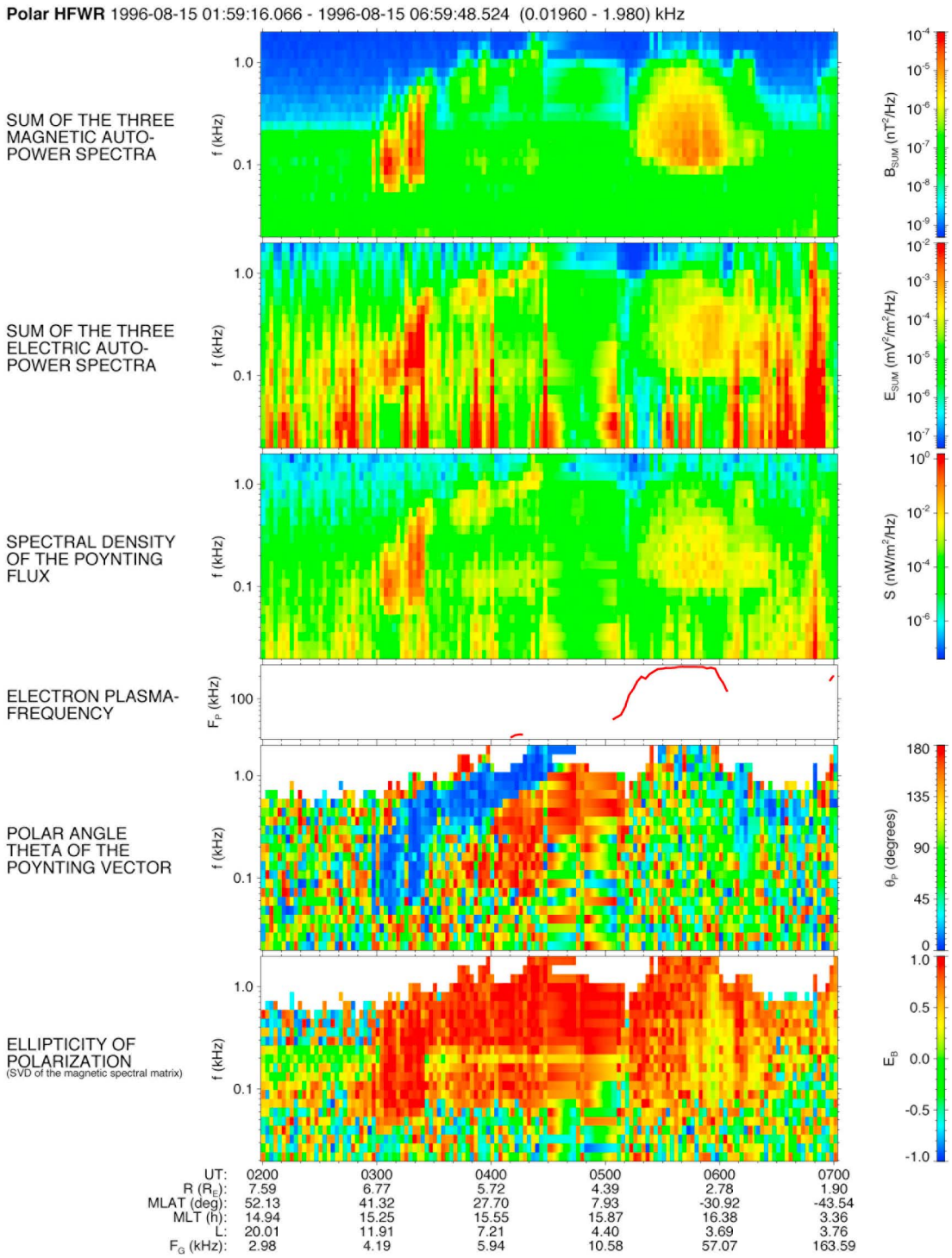

Figure 7. An example of Polar plasma waves and the measured properties available for statistical studies. The details of various panels are given in the text. One particularly interesting feature of the waves is given in the second panel from the bottom, the Poynting vector relative to the magnetic field direction. There are blue (downgoing) and red (upcoming) waves present in adjacent areas.

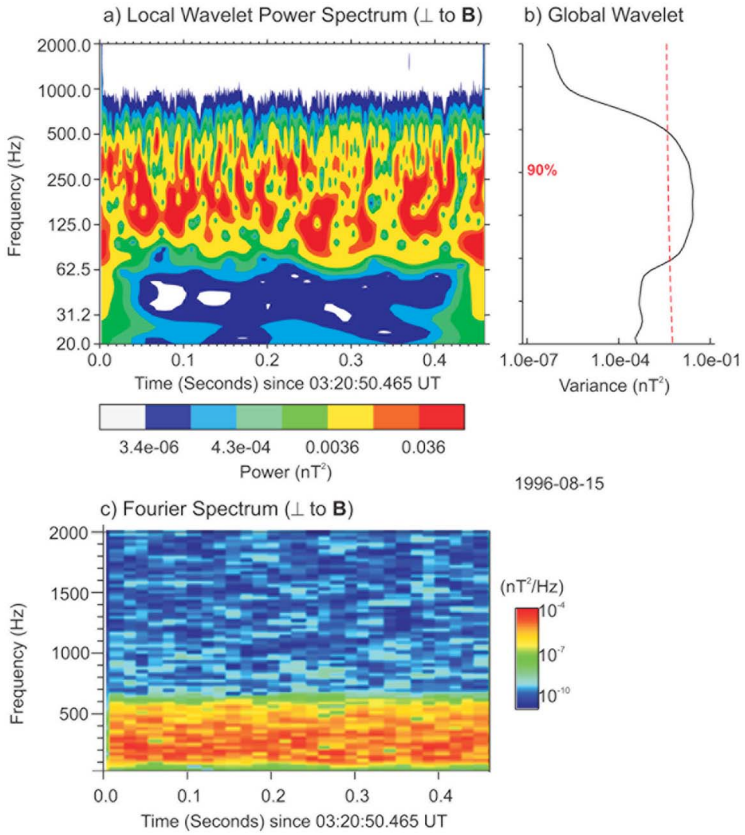

Figure 8. Wavelet analysis for the downgoing (blue) waves of Figure 7 between ~03:20:50 and ~03:20:50 UT. (a) The local wavelet power spectrum at each of 2048 points covering 459 ms. (b) The global (time-averaged) wavelet power spectrum with the red dashed line indicating the 90% confidence level. The most intense chorus emissions are observed in the ~100–500 Hz band. (c) A Fourier spectrum of the waves.

are detected well outside of the plasmasphere, in the outer magnetosphere. The waveform data for this interval is shown later in the paper (Figure 9). An example of chorus in the generation region (Figure 15) is also shown for comparative purposes. These figures will be discussed in more detail later in the paper.

[27] Figure 8b shows the global wavelet analysis of the ~0.5 s of data shown in Figure 8a. The global wavelet spectrum is a measure of the time-averaged wavelet spectrum over all the local spectra for the entire interval and is an efficient estimator of the true power spectrum, providing the variance of power over frequency. The red-dashed line provides the 90% confidence level, using a chi-square distribution, when compared to a Fourier power spectrum (white noise) at each scale (frequency). The average power over the interval is $\sim 10^{-2}$ nT^2. It is noted that the average power level shown here is near the peak chorus power (determined by power spectra) detected in the equatorial generation region [*Tsurutani and Smith*, 1977].

[28] Figure 9 shows the magnetic field components (top three panels) given in minimum variance coordinates. The time interval for Figure 9 is the same as in Figure 8. Standard notation is used where B1, B2 and B3 correspond to the maximum, intermediate and minimum variance directions [*Sonnerup and Cahill*, 1967]. This system is a right-handed one where B1 × B2 = B3. Examination of electromagnetic waves using a minimum variance technique has several advantages. It is known that the magnetic perturbation of the waves is orthogonal to the direction of the wave phase velocity [*Storey*, 1959; *Verkhoglyadova and Tsurutani*, 2009; *Verkhoglyadova et al.*, 2009, 2010], thus the wave k direction (phase velocity direction) lies along the B3 (the minimum variance) direction. The relationship between the two wave transverse components (B1 and B2) defines both the wave ellipticity and the sense of rotation [*Smith and Tsurutani*, 1976]. By plotting B1 versus B2 over time (called a hodogram), both of the latter quantities/qualities can be obtained. All of the above wave properties are needed to correctly assess the wave mode and thus potential wave-particle interactions.

[29] The top two panels of Figure 9 show about equal amplitude fluctuations in B1 and B2 (maximum and intermediate variance directions) and minimum amplitude fluctuations in the B3 panel. There were ~3 distinct, coherent cycles present at time ~0.05 s in the B1 and B2 panels. Other coherent intervals can be found at ~0.10 s and ~0.20 s. The peak amplitudes were ~0.1 to 0.15 nT. This is slightly greater than the "average" value shown in Figure 8b. The other waves present in the interval often lack the nice periodicity that is present in these three cycle clusters.

[30] The bottom left B1-B2 hodogram indicates that the waves were nearly circularly polarized. The bottom right B1-B3 hodogram shows that the waves were close to planar structures. Of course this result is for a mix of waves propa-

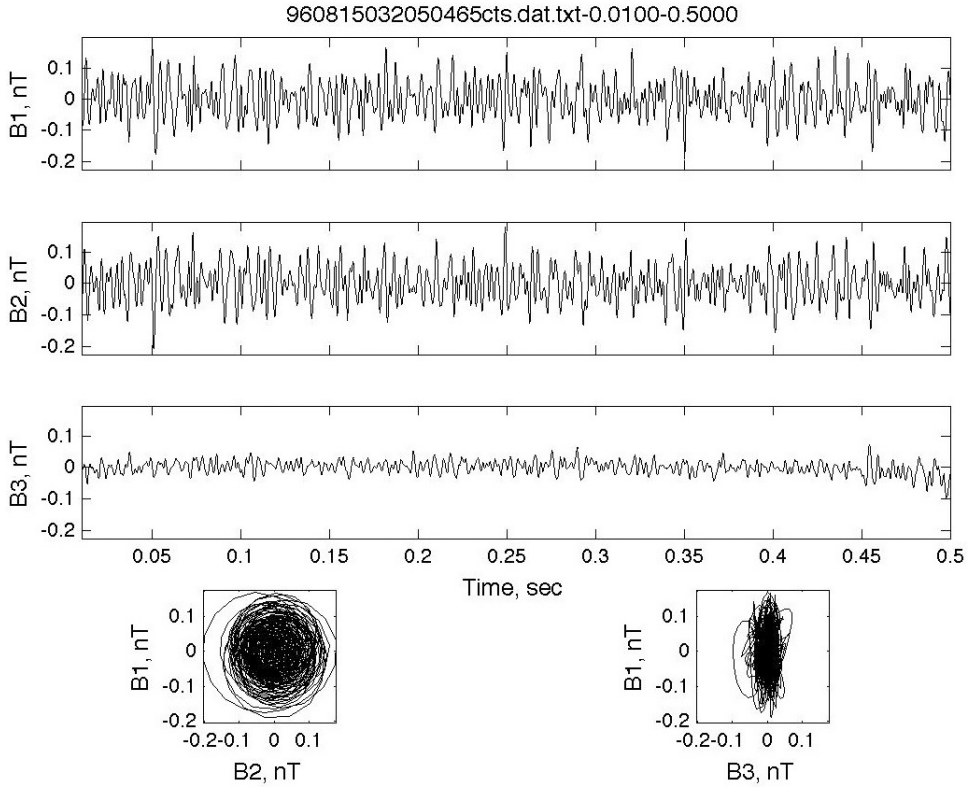

Figure 9. The chorus interval of Figure 8 (03:20:50–03:20:50 UT) in minimum variance coordinates. B1, B2, and B3 are the field components in the maximum, intermediate, and minimum variance directions.

gating at different angles from each other. The waves may be coming from different sources in the magnetosphere.

[31] Figure 10 gives an example of the polarization of chorus. A single cycle of the wave is shown in minimum variance coordinates. From top to bottom are the three magnetic field components and two hodograms, B1 versus B2 and B1 versus B3. In the hodogram a triangle indicates the beginning of the interval. The coordinate system is right-

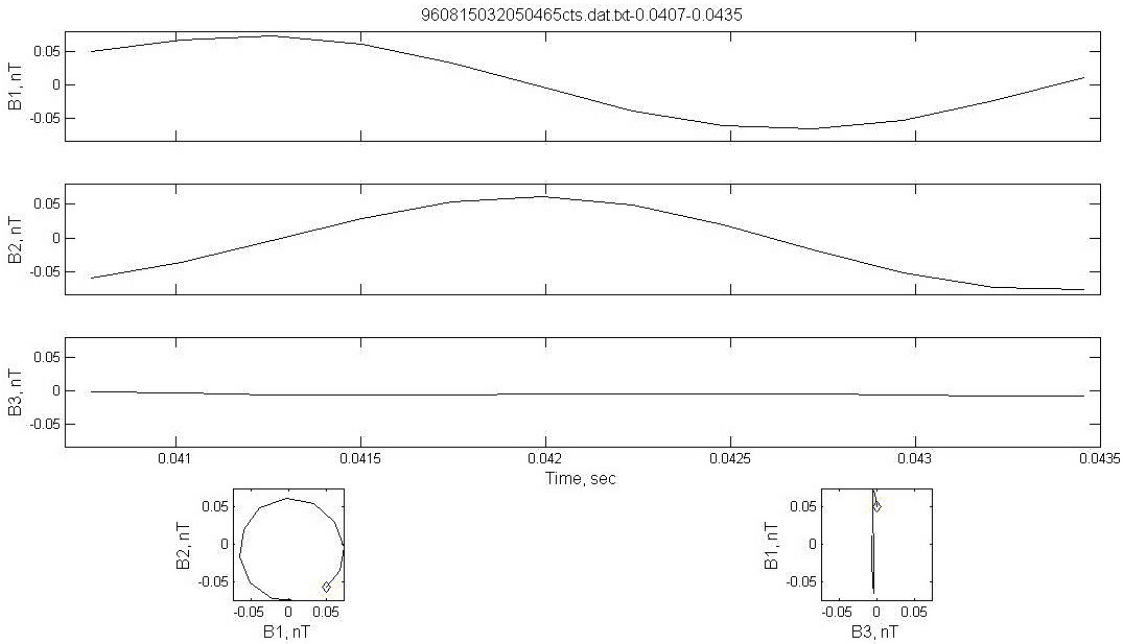

Figure 10. An example of a single cycle of chorus taken at ~03:20:51 UT on 15 August 1996. This is taken near the start of the Figure 8 interval.

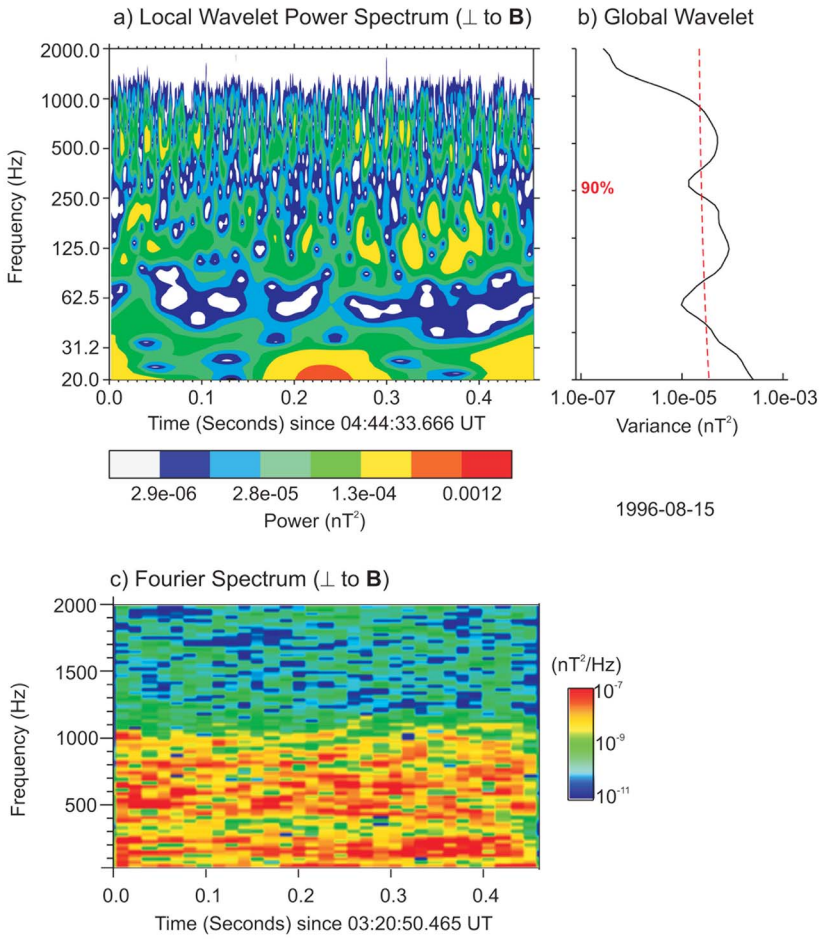

Figure 11. Wavelet analysis for the upcoming (red) waves of Figure 7 between ~04:44:33 and ~04:44:34 UT. Same format as Figure 8. The chorus emissions are observed at ~500 Hz.

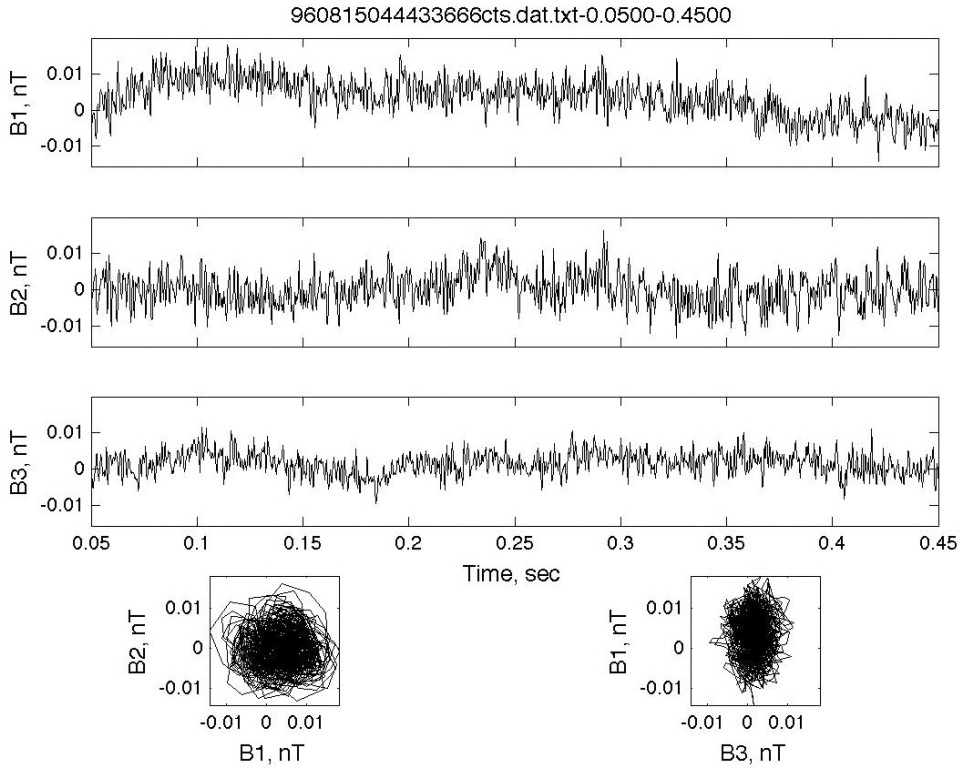

Figure 12. Same format as Figure 9. The time interval is the same as Figure 11. These are the upcoming (red) waves at ~04:44 UT.

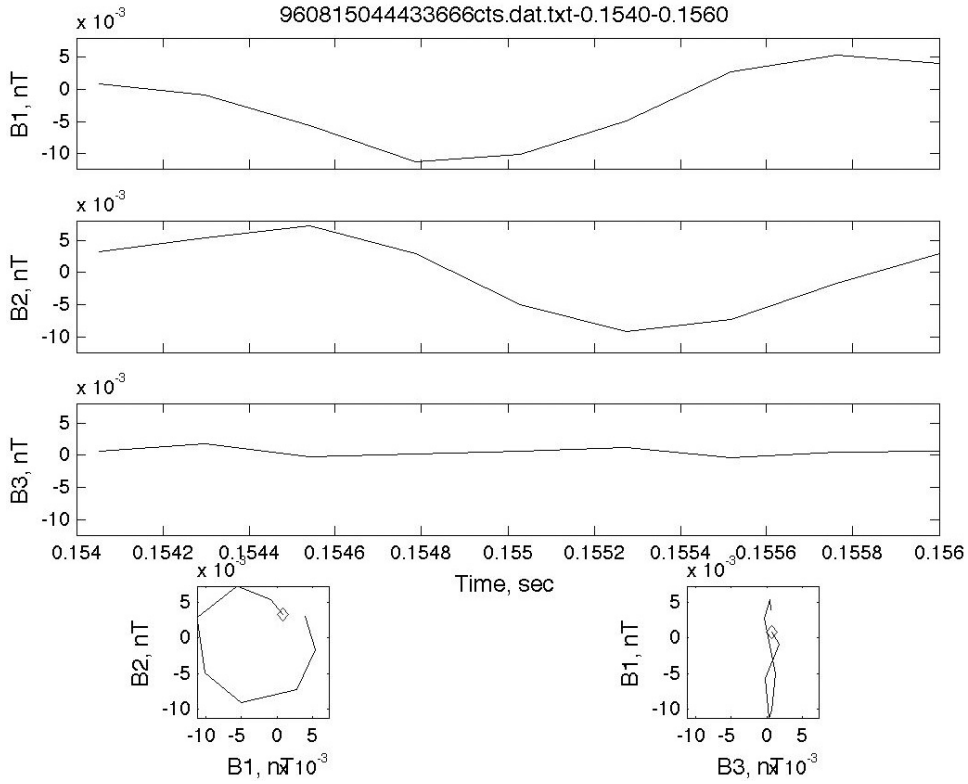

Figure 13. Same format as Figure 10 except for ~04:44 UT.

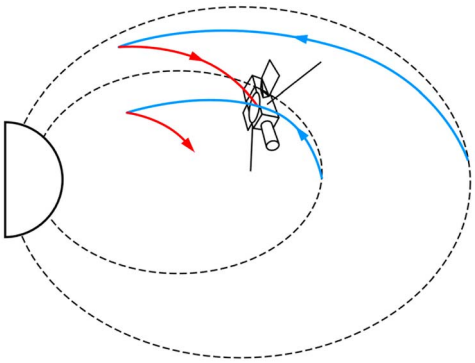

Figure 14. A schematic of the relationship between the downgoing (blue) and upcoming (red) chorus. Two possible routes of the waves from their generation region to the spacecraft are shown.

handed and B_0 is out of the paper in the general direction of B3. The bottom left panel thus shows that the wave was right-hand circularly polarized as expected for whistler mode chorus. The wave phase direction of propagation was ~8° relative to B_0. The bottom right hodogram shows that the wave was planar (the B3 variation is small relative to B1).

[32] Figure 11 provides the wavelet analysis of the waves at ~04:44:34 UT. This interval corresponds to the upcoming (red) waves in Figure 7. The chorus waves can be noticed by the short-duration bursts at ~500 Hz in Figure 11a. The average power as shown in Figure 11b is $\sim 10^{-4}$ nT^2. Thus in this example of upcoming waves, the wave power was roughly 2 orders of magnitude less than the Figure 7 downgoing waves. Again there were no indications that the upcoming waves were composed of coherent elements as typically detected closer to the generation region.

[33] Figure 12 shows the Figure 11 interval magnetic field in minimum variance coordinates. The B1 and B2 fluctuation values were approximately equal and slightly higher than the B3 values. The peak amplitudes in the B1 and B2 components just after 0.1 s was ~0.007 nT. This value is consistent with the average power in Figure 11b. The level of wave coherence here is less than that of the downgoing waves shown earlier. A few single wave cycles can be seen at time ~0.1 s, but multiple cycles are absent throughout the interval.

[34] The hodograms indicate the waves were somewhat circularly polarized (left panel) and somewhat planar (right panel). There was a significant difference of these upgoing waves from the downgoing ones.

[35] Figure 13 gives hodograms for a single wave cycle at 04:44:33 UT. The ambient magnetic field direction is out of the paper. The wave is right-hand circularly polarized and planar. The wave is found to be propagating at ~37° relative to B_0. Other intervals adjacent to this cycle were analyzed in a similar fashion. The intervals were found to contain transverse waves with varying amplitudes and angles of propagation relative to B_0.

4. Summary and Discussion

[36] The study was done using Polar plasma wave data taken during the minimum of the solar cycle, between SC 22 and SC 23. The geomagnetic *Dst* and *AE* indices and the solar wind ram pressure were low during the study (Figures 4, 5 and 6). There was a lack of chorus/EM waves detected inside of L* = 4. This is consistent with a general lack of intense magnetic storms occurring during the interval of study. With a lack of intense storm-time electric fields to convect the plasma sheet electrons deep into the magnetosphere, anisotropic electrons and chorus will not be present in this portion of the magnetosphere.

[37] There was an asymmetry in the chorus spatial location, with most events occurring prenoon (Figure 2). This is consistent with local generation of chorus by anisotropic and energetic ~5 to 100 keV substorm electrons drifting from midnight through dawn to noon and a loss of electron free energy for instability postnoon [see also *Tsurutani and Smith*, 1977; *Meredith et al.*, 2001]. The preponderance of chorus occurring when -40 nT < *Dst* < 0 nT (Figure 4) and a preference for high *AE* values (Figure 5) are in support of a substorm/weak storm source for some chorus events.

[38] There is also an indication of chorus dependence on high solar wind pressure (Figure 6). These chorus events could be caused by a mechanism of compression of preexisting outer zone dayside energetic ~5 to 100 keV electrons and the loss cone instability associated with this compression [*Zhou and Tsurutani*, 1999; *Tsurutani et al.*, 2001].

[39] The results indicating several causes of the dayside outer zone chorus are not new [*Tsurutani and Smith*, 1977; *Horne et al.*, 2005b]. However, the identification of chorus sometimes occurring during low solar wind pressure (Figure 6) is new and is a surprise to the authors. One speculation is that these chorus events could be associated with solar wind pressure decreases. Such pressure decreases would decompress preexisting outer zone energetic electrons leading to a $T_{\|}/T_{\perp} > 1$ anisotropy. This electron anisotropy has been suggested to lead to Gendrin mode chorus wave growth via a Landau instability [*Gendrin*, 1961; *Helliwell*, 1995; *Verkhoglyadova and Tsurutani*, 2009; *Verkhoglyadova et al.*, 2009, 2010]. Case studies will be needed to examine this possibility in detail.

[40] A typical Polar pass of dayside outer zone chorus was studied (Figure 7). A common characteristic found was simultaneous downgoing (blue) waves and upcoming (red) waves at lower frequencies. Similar statistical results were shown in Figure 4b of *Santolík et al.* [2010b]. These two sets of waves were studied in detail. The downgoing waves were found to have intensities of $\sim 10^{-2}$ nT^2 and were quasi-coherent (lacking the coherence of subelements noted by *Santolík et al.* [2003, 2004], *Verkhoglyadova et al.* [2009] and *Tsurutani et al.* [2009]). There are instances where the waves have a few consecutive cycles of coherent right-hand circular polarization (Figures 8, 9 and 10). The upcoming (red) waves had intensities of $\sim 10^{-4}$ nT^2 and were again quasi-coherent but contained only single cycles of right-hand circular polarization (Figures 11, 12 and 13).

[41] Figure 14 gives a schematic of wave propagation within the magnetosphere that attempts to explain the above observations. We assume wave generation at the magnetic equator [*Tsurutani and Smith*, 1974; *LeDocq et al.*, 1998; *Lauben et al.*, 2002]. Two sample wave trajectories are shown. Both waves propagate inward (downward) toward lower L*, consistent with previous ray tracing results [*Chum and Santolík*, 2005; *Santolík et al.*, 2006; *Bortnik et al.*, 2008]. The outermost wave propagates downward to low altitudes

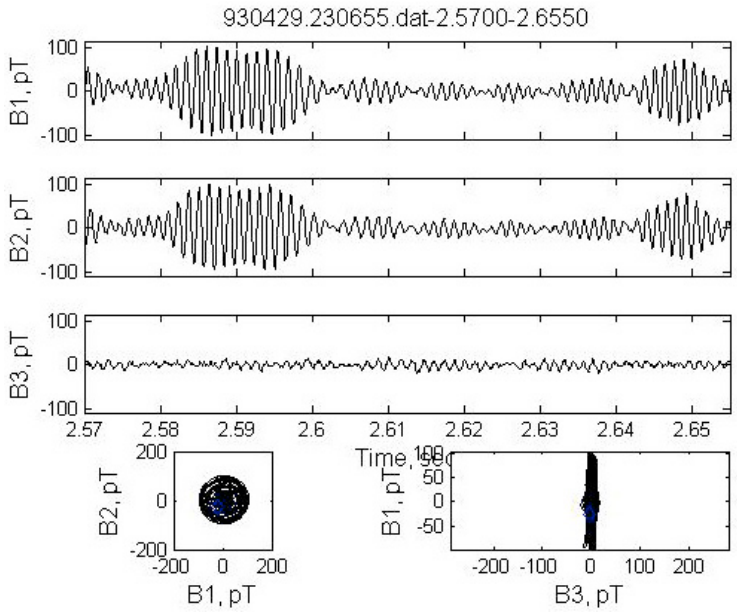

Figure 15. An example of a ~0.1 s chorus element taken from Geotail data. The data are shown in minimum variance coordinates. The B1-B2 and B1-B3 hodograms are shown at the bottom. The element is composed of many coherent subelements.

and then is refracted back upward away from the Earth. The same is true for the innermost wave. For easy visualization, inward going waves are colored blue and refracted waves red, respectively. This schematic shows that the Polar spacecraft could possibly detect a wave whose source is located at the equator but at higher L* (the red wave reaching the spacecraft as shown in Figure 14). This wave would propagate to low altitudes and then reflect back out [*Parrot et al.*, 2003, 2004; *Santolík et al.*, 2010b]. Because the wave was generated at a large L* and traveled a greater distance to reach Polar, the greater Landau damping due to its longer path will lead to a lower intensity at Polar.

[42] Does this scenario match the observations of Figure 7? In the Figure, it is noted that when blue (downgoing) and red (upgoing) chorus occurs simultaneously, the blue chorus is at higher frequencies than the red chorus. Assuming that the waves are generated at a fraction of the electron cyclotron frequency (typically ~0.25 to 0.5 f_{ce}), the refracted red waves will be at a lower frequency. This is one explanation why the more intense downgoing blue waves are at higher frequencies than the upcoming red waves. Thus in general, the schematic in Figure 14 is consistent with the observations.

[43] The Polar observations show a new feature of chorus. At distances away from the equatorial generation region, chorus is only quasi-coherent in nature (Figures 8 through 13). The coherent ~10 to 100 ms chorus subelements noted by *Santolík et al.* [2004], *Verkhoglyadova et al.* [2009] and *Tsurutani et al.* [2009] are not present. For comparative purposes, Figure 15 shows an example of coherent chorus subelements (taken from the work of *Tsurutani et al.* [2009]). The magnetic field components are given in minimum variance coordinates similar to what was shown in Figures 9 and 12. This interval shows a ~0.1 s duration chorus rising tone "element." The chorus was detected in a dayside outer zone minimum B pocket with peak amplitudes of ~0.2 nT at a center frequency of ~700 Hz. This element is composed of several coherent subelements or "packets" [*Santolík et al.*, 2003]. The subelement durations range from ~0.01 to ~0.02 s. Low-intensity isotropic incoherent noise (~0.20 pT) separates the subelements [*Tsurutani et al.*, 2009]. This waveform is substantially different from the roughly constant amplitude downward propagating or upward propagating chorus shown earlier. The chorus wave amplitude is highly variable (a typical feature of chorus in the generation region). Second, the B1 and B2 components stay in relative constant phase with each other over many cycles.

[44] These coherent chorus subelements have been theorized by *Lakhina et al.* [2010] to cause very rapid pitch angle scattering, leading to ionospheric microbursts [*Anderson and Milton*, 1964]. However, the chorus observed by Polar away from the equatorial generation region is only quasi-coherent, and the recent results of *Lakhina et al.* [2010], which are based on resonant interaction of electrons with coherent chorus waves, are not directly applicable. Similarly, quasi-linear diffusion theories [*Kennel and Petschek*, 1966; *Summers et al.*, 2007a, 2007b] based on incoherent waves also cannot accurately describe the wave-particle interaction of quasi-coherent chorus interacting with electrons. There is a need to develop a new theory for the wave-particle interactions between electrons and the quasi-coherent off-equatorial region chorus.

[45] The quasi-coherent chorus waves are not totally "turbulent" like plasmaspheric hiss, but are composed of single cycles of right-hand circularly polarized waves. How this feature develops physically is not known at this time. It is possible that wave dispersion may lead to this quasi-coherent state. Propagation from multiple sources to the point of observation is another possibility. In addition, wave-wave interactions cannot be ruled out either at this time.

[46] Is there a way to quantitatively examine the coherence level of chorus? Figure 16 is an attempt to do this. The Figure shows the B1-B2 components of chorus for ~0.02 s of the

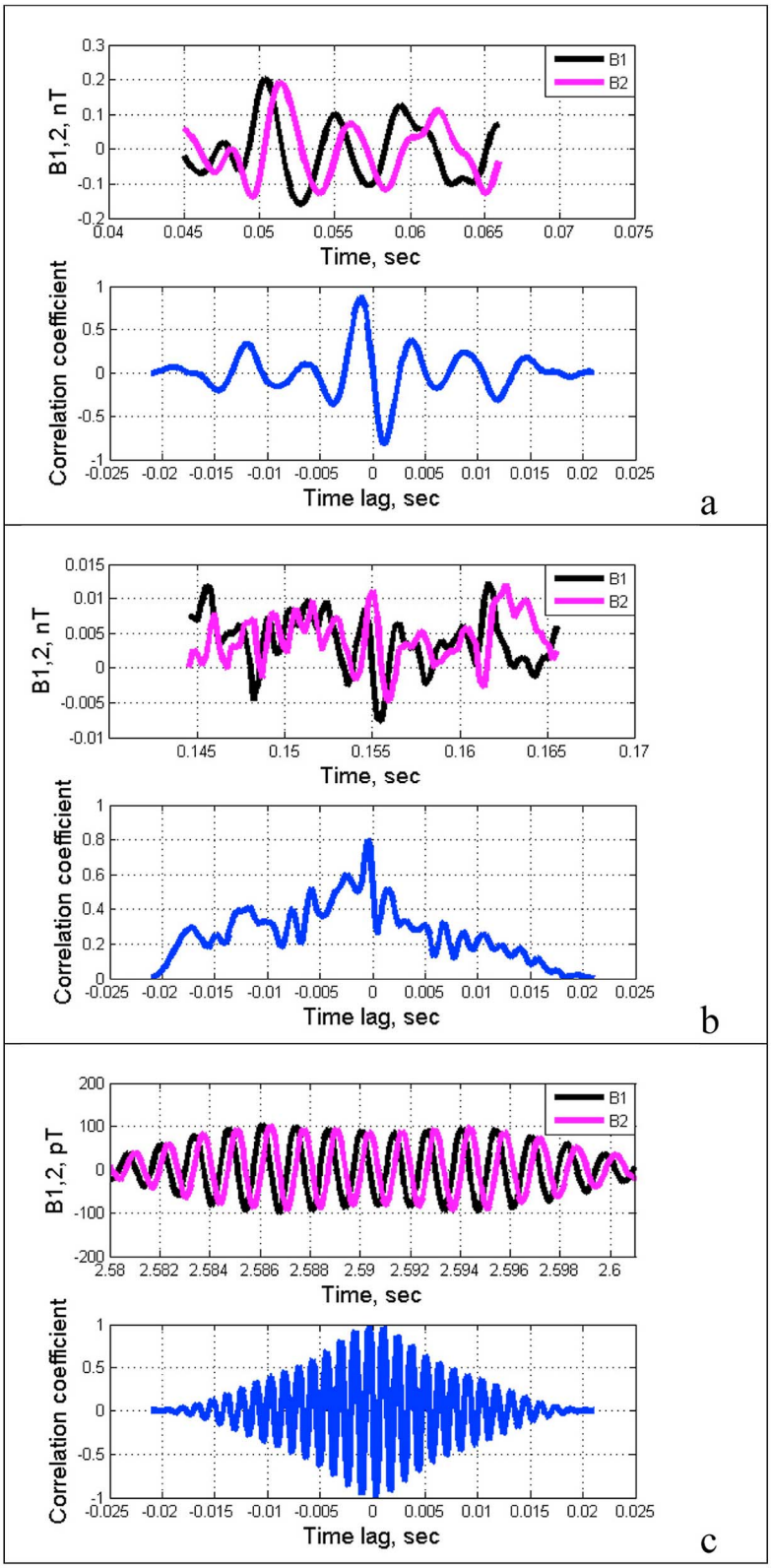

Figure 16. The B1-B2 components for (a) Polar downgoing chorus, (b) Polar upcoming chorus, and (c) Geotail chorus in the generation region. The top figures of the panels show B1 and B2 versus time, and the bottom figures show the cross-correlation analyses between B1 and B2. The correlation coefficient at zero lag and 1-wave, 2-wave, etc., lags indicate the wave coherency. Geotail chorus (Figure 16c) has the highest level of coherency, followed by downgoing waves detected at Polar, and the least coherent waves being the Polar upcoming chorus.

high-resolution magnetic field data of the Polar downgoing (Figure 16a), Polar upcoming (Figure 16b) and Geotail generation region chorus (Figure 16c). In each of the three panels, the top figures show B1 and B2 values as a function of time. The bottom figures show the B1-B2 cross correlation results. The data used were taken from ~0.02 s intervals from data from Figures 9, 12 and 15. The specific times were 0.045 to 0.066 s, 0.1445 to 0.1655 s (both reference times are from 03:20:50 UT and 04:44:33 UT, on 15 August 1996) and ~23:06:20 UT 29 April 1993, respectively. For the downgoing waves (Figure 16a), the peak correlation coefficient is ~0.9 with the first side lobe amplitude ~0.4. For the upcoming waves (Figure 16b) the peak correlation coefficient is ~0.55 (an average of 0.8 and 0.3) with the first side lobe amplitude of ~0.5. For the generation region chorus (Figure 16c), the peak correlation coefficient is ~1.0 with the first side lobe peak coefficient ~0.95. The cross correlation amplitudes indicate the coherency of the waves. Thus the generation region Geotail waves have the highest coherency, the downgoing waves detected away from the generation region are less coherent, and the upcoming waves are the least coherent of the three. The wave amplitudes decrease in the same order, as expected.

5. Final Comments

[47] The Polar results are consistent with magnetospheric right-hand circularly polarized chorus reflecting at low altitudes and propagating back toward the magnetic equator as an upcoming wave. The reflected chorus is lower in intensity by ~2 orders of magnitude. This is in good agreement with previous ray tracing studies [*Chum and Santolík*, 2005; *Santolík et al.*, 2006; *Bortnik et al.*, 2008, 2009]. These intensities should be compared with models and can be used in wave-particle interaction calculations/models to study electron pitch angle scattering (and loss) as well as for electron acceleration.

[48] How are relativistic microbursts [*Lorentzen et al.*, 2001a, 2001b] produced? These electron precipitation events have approximately the same rapid timescales as the lower energy ~5–100 keV electron microbursts. One possibility is electron cyclotron interaction with higher harmonics of the chorus subelements. However, in this mechanism the resonant wave amplitudes will be less and the particle rigidity greater, so further calculations are necessary to determine if this mechanism is feasible or not. Other previously proposed possibilities are off-equatorial cyclotron resonant interaction mechanisms, modified by the reduced chorus coherence (and amplitude) shown here. A defining experimental observation that can distinguish between the several possibilities is to determine the relationship between low-energy microbursts and relativistic microbursts. If different energy microbursts are found to be initiated at the same time, then it is quite likely that a single pitch angle scattering mechanism is generating both types.

[49] A Fourier spectrum of chorus detected far from the generation region appears similar to broadbanded "hiss" (Figure 8c). This is not a new observation, as many chorus researchers have noted this before. We refer the reader to the work of *Tsurutani and Smith* [1974, Figures 1–3] and *Goldstein and Tsurutani* [1984, Figures 14, 16, and 17] for examples of "hiss" in the outer magnetosphere. One difference of the above "hiss" examples is that they were observed near the magnetic equator. Thus for the cases where there is chorus triggered by a "hiss" band (Figures 16 and 17 from the work of *Goldstein and Tsurutani* [1984]), the "hiss" maybe semicoherent chorus that has propagated from a more distant source.

[50] The most difficult case, but probably the most interesting from a physical point of view, is Figure 3 from the work of *Tsurutani and Smith* [1974]. 5–15 s quasiperiodic hiss was found to trigger time delayed, higher frequency ~5–15 s quasiperiodic falling tone chorus. The physics of falling tone chorus elements alone has been difficult for theorists, but time delayed, triggered, higher-frequency emissions are an even greater challenge. Actually the basic physics of the ~5–15 s quasiperiodicities of the waves (and concomitant ~5–15 s auroral patches) has never been solved, to the authors' knowledge.

[51] **Acknowledgments.** Portions of this research were carried out at the Jet Propulsion Laboratory, California Institute of Technology, under contract with NASA. G.S.L. thanks the Indian National Science Academy, New Delhi, for the support under the Senior Scientist Scheme. J.S.P. and O.S. acknowledge JPL support under subcontract 1246597. O.S. acknowledges additional support from grants GACR 205/10/2279 and ME10001. B.T.T. acknowledges the Technical University of Braunschweig (TUB) for their hospitality during his sabbatical in the summer of 2010. Portions of the revisions to this paper were written during his stay at TUB. We thank E. Echer of INPE for help with the geomagnetic indices. We thank D. Boscher for maintaining the ONERA-DESP library that was used to calculate the L* values.

[52] Robert Lysak thanks the reviewers for their assistance in evaluating this paper.

References

Albert, J. M. (2002), Nonlinear interaction of outer zone electrons with VLF waves, *Geophys. Res. Lett.*, *29*(8), 1275, doi:10.1029/2001GL013941.

Anderson, K. A., and D. W. Milton (1964), Balloon observations of X rays in the auroral zone: 3. High time resolution studies, *J. Geophys. Res.*, *69*, 4457–4479, doi:10.1029/JZ069i021p04457.

Anderson, R. R., and K. Maeda (1977), VLF emissions associated with enhanced magnetospheric electrons, *J. Geophys. Res.*, *82*, 135–146, doi:10.1029/JA082i001p00135.

Bortnik, J., R. M. Thorne, and N. P. Meredith (2008), The unexpected origin of plasmaspheric hiss from discrete chorus emissions, *Nature*, *452*, 62–66, doi:10.1038/nature06741.

Bortnik, J., R. M. Thorne, and N. P. Meredith (2009), Plasmaspheric hiss overview and relation to chorus, *J. Atmos. Sol. Terr. Phys.*, *71*, 1636–1646.

Burtis, W. J., and R. A. Helliwell (1969), Banded chorus—A new type of VLF radiation observed in the magnetosphere by OGO 1 and OGO 3, *J. Geophys. Res.*, *74*, 3002–3010, doi:10.1029/JA074i011p03002.

Burtis, W. J., and R. A. Helliwell (1976), Magnetospheric chorus: Occurrence patterns and normalized frequency, *Planet. Space Sci.*, *24*, 1007–1010, doi:10.1016/0032-0633(76)90119-7.

Burton, R. K., and R. E. Holzer (1974), The origin and propagation of chorus in the outer magnetosphere, *J. Geophys. Res.*, *79*, 1014–1023, doi:10.1029/JA079i007p01014.

Chum, J., and O. Santolík (2005), Propagation of whistler-mode chorus to low altitudes: Divergent ray trajectories and ground accessibility, *Ann. Geophys.*, *23*, 3727–3738, doi:10.5194/angeo-23-3727-2005.

Cornilleau-Wehrlin, N., R. Gendrin, F. Lefeuvre, M. Parrot, R. Grard, D. Jones, A. Bahnsen, E. Ungstrup, and W. Gibbons (1978), VLF electromagnetic waves observed onboard GEOS-1, *Space Sci. Rev.*, *22*, 371–382, doi:10.1007/BF00210874.

Gendrin, R. (1961), Le guidage des whistlers par le champ magnetique, *Planet. Space Sci.*, *5*, 274–278, doi:10.1016/0032-0633(61)90096-4.

Goldstein, B. E., and B. T. Tsurutani (1984), Wave normal directions of chorus near the equatorial source region, *J. Geophys. Res.*, *89*, 2789–2810, doi:10.1029/JA089iA05p02789.

Gonzalez, W. D., J. A. Joselyn, Y. Kamide, H. W. Kroehl, G. Rostoker, B. T. Tsurutani, and V. M. Vasyliūnas (1994), What is a geomagnetic storm?, *J. Geophys. Res.*, *99*, 5771–5792, doi:10.1029/93JA02867.

Gurnett, D. A., and B. J. O'Brien (1964), High-latitude geophysical studies with satellite Injun 3: 5. Very-low-frequency electromagnetic radiation, *J. Geophys. Res.*, *69*, 65–89, doi:10.1029/JZ069i001p00065.

Gurnett, D. A., et al. (1995), The Polar plasma wave instrument, *Space Sci. Rev.*, *71*, 597–622, doi:10.1007/BF00751343.

Haque, N., M. Spasojevic, O. Santolík, and U. S. Inan (2010), Wave normal angles of magnetospheric chorus emissions observed on the Polar spacecraft, *J. Geophys. Res.*, *115*, A00F07, doi:10.1029/2009JA014717.

Helliwell, R. A. (1995), The role of the Gendrin mode of VLF propagation in the generation of magnetospheric emissions, *Geophys. Res. Lett.*, *22*, 2095–2098, doi:10.1029/95GL02003.

Hikishima, M., Y. Omura, and D. Summers (2010), Microburst precipitation of energetic electrons associated with chorus wave generation, *Geophys. Res. Lett.*, *37*, L07103, doi:10.1029/2010GL042678.

Horne, R. B., and R. M. Thorne (1998), Potential waves for relativistic electron scattering and stochastic acceleration during magnetic storms, *Geophys. Res. Lett.*, *25*, 3011–3014, doi:10.1029/98GL01002.

Horne, R. B., N. P. Meredith, R. M. Thorne, D. Heynderickx, R. H. A. Iles, and R. R. Anderson (2003a), Evolution of energetic electron pitch angle distributions during storm time electron acceleration to megaelectronVolt energies, *J. Geophys. Res.*, *108*(A1), 1016, doi:10.1029/2001JA009165.

Horne, R. B., S. A. Glauert, and R. M. Thorne (2003b), Resonant diffusion of radiation belt electrons by whistler-mode chorus, *Geophys. Res. Lett.*, *30*(9), 1493, doi:10.1029/2003GL016963.

Horne, R. B., et al. (2005a), Wave acceleration of electrons in the Van Allen radiation belts, *Nature*, *437*, 227–230, doi:10.1038/nature03939.

Horne, R. B., R. M. Thorne, S. A. Glauert, J. M. Albert, N. P. Meredith, and R. R. Anderson (2005b), Timescale for radiation belt electron acceleration by whistler mode chorus waves, *J. Geophys. Res.*, *110*, A03225, doi:10.1029/2004JA010811.

Inan, U. S. (1987), Gyroresonant pitch angle scattering by coherent and incoherent whistler mode waves in the magnetosphere, *J. Geophys. Res.*, *92*, 127–142, doi:10.1029/JA092iA01p00127.

Inan, U. S., T. F. Bell, and R. A. Helliwell (1978), Nonlinear pitch angle scattering of energetic electrons by coherent VLF waves in the magnetosphere, *J. Geophys. Res.*, *83*, 3235–3253, doi:10.1029/JA083iA07p03235.

Inan, U. S., Y. T. Chiu, and G. T. Davidson (1992), Whistler-mode chorus and morningside aurorae, *Geophys. Res. Lett.*, *19*, 653–656, doi:10.1029/92GL00402.

Kennel, C. F., and H. E. Petschek (1966), Limit on stably trapped particle fluxes, *J. Geophys. Res.*, *71*, 1–28.

Koons, H. C., and J. L. Roeder (1990), A survey of equatorial magnetospheric wave activity between 5 and 8 R_E, *Planet. Space Sci.*, *38*, 1335–1341, doi:10.1016/0032-0633(90)90136-E.

Lakhina, G. S., B. T. Tsurutani, O. P. Verkhoglyadova, and J. S. Pickett (2010), Pitch angle transport of electrons due to cyclotron interactions with the coherent chorus subelements, *J. Geophys. Res.*, *115*, A00F15, doi:10.1029/2009JA014885.

Lauben, D. S., U. S. Inan, T. F. Bell, and D. A. Gurnett (2002), Source characteristics of ELF/VLF chorus, *J. Geophys. Res.*, *107*(A12), 1429, doi:10.1029/2000JA003019.

LeDocq, M. J., D. A. Gurnett, and G. B. Hospodarsky (1998), Chorus source locations from VLF Poynting flux measurements with the Polar spacecraft, *Geophys. Res. Lett.*, *25*, 4063–4066, doi:10.1029/1998GL900071.

Lorentzen, K. R., J. B. Blake, U. S. Inan, and J. Bortnik (2001a), Observations of relativistic electron microbursts in association with VLF chorus, *J. Geophys. Res.*, *106*, 6017–6027, doi:10.1029/2000JA003018.

Lorentzen, K. R., M. D. Looper, and J. B. Blake (2001b), Relativistic electron microbursts during the GEM storms, *Geophys. Res. Lett.*, *28*, 2573–2576, doi:10.1029/2001GL012926.

McIlwain, C. E. (1961), Coordinates for mapping the distribution of magnetically trapped particles, *J. Geophys. Res.*, *66*, 3681–3691, doi:10.1029/JZ066i011p03681.

Meredith, N. P., R. B. Horne, and R. R. Anderson (2001), Substorm dependence of chorus amplitudes: Implications for the acceleration of electrons to relativistic energies, *J. Geophys. Res.*, *106*, 13,165–13,178, doi:10.1029/2000JA900156.

Meredith, N. P., R. B. Horne, R. H. A. Iles, R. M. Thorne, D. Heynderickx, and R. R. Anderson (2002), Outer zone relativistic electron acceleration associated with substorm enhanced whistler mode chorus, *J. Geophys. Res.*, *107*(A7), 1144, doi:10.1029/2001JA900146.

Meredith, N. P., M. Cain, R. B. Horne, R. M. Thorne, D. Summers, and R. R. Anderson (2003), Evidence for chorus-driven electron acceleration to relativistic energies from a survey of geomagnetically disturbed periods, *J. Geophys. Res.*, *108*(A6), 1248, doi:10.1029/2002JA009764.

Nakamura, R., M. Isowa, Y. Kamide, D. N. Baker, J. B. Blake, and M. Looper (2000), SAMPEX observations of precipitation bursts in the outer radiation belt, *J. Geophys. Res.*, *105*, 15,875–15,885, doi:10.1029/2000JA900018.

Omura, Y., and D. Summers (2006), Dynamics of high-energy electrons interacting with whistler mode chorus emissions in the magnetosphere, *J. Geophys. Res.*, *111*, A09222, doi:10.1029/2006JA011600.

Omura, Y., N. Furuya, and D. Summers (2007), Relativistic turning acceleration of resonant electrons by coherent whistler mode waves in a dipole magnetic field, *J. Geophys. Res.*, *112*, A06236, doi:10.1029/2006JA012243.

Omura, Y., Y. Katoh, and D. Summers (2008), Theory and simulation of the generation of whistler-mode chorus, *J. Geophys. Res.*, *113*, A04223, doi:10.1029/2007JA012622.

Parks, G. K. (1967), Spatial characteristics of aurora-zone X-ray microbursts, *J. Geophys. Res.*, *72*, 215–226, doi:10.1029/JZ072i001p00215.

Parks, G. K., and J. R. Winckler (1969), Simultaneous observations of 5- to 15-second period modulated energetic electron fluxes at the synchronous altitude and the auroral zone, *J. Geophys. Res.*, *74*, 4003–4017, doi:10.1029/JA074i016p04003.

Parrot, M., O. Santolík, N. Cornilleau-Wehrlin, M. Maksimovic, and C. C. Harvey (2003), Magnetospherically reflected chorus waves revealed by ray tracing with Cluster data, *Ann. Geophys.*, *21*, 1111–1120, doi:10.5194/angeo-21-1111-2003.

Parrot, M., O. Santolík, D. A. Gurnett, J. S. Pickett, and N. Cornilleau-Wehrlin (2004), Characteristics of magnetospherically reflected chorus waves observed by Cluster, *Ann. Geophys.*, *22*, 2597–2606, doi:10.5194/angeo-22-2597-2004.

Roederer, J. G. (1970), *Dynamics of Geomagnetically Trapped Radiation*, *Phys. Chem. Space*, vol. 2, Springer, Berlin.

Roth, I., M. A. Temerin, and M. K. Hudson (1999), Resonant enhancement of relativistic electron fluxes during geomagnetically active periods, *Ann. Geophys.*, *17*, 631–638, doi:10.1007/s00585-999-0631-2.

Santolík, O., D. A. Gurnett, J. S. Pickett, M. Parrot, and N. Cornilleau-Wehrlin (2003), Spatio-temporal structure of storm-time chorus, *J. Geophys. Res.*, *108*(A7), 1278, doi:10.1029/2002JA009791.

Santolík, O., D. A. Gurnett, J. S. Pickett, M. Parrot, and N. Cornilleau-Wehrlin (2004), A microscopic and nanoscopic view of storm-time chorus on 31 March, 2001, *Geophys. Res. Lett.*, *31*, L02801, doi:10.1029/2003GL018757.

Santolík, O., J. Chum, M. Parrot, D. A. Gurnett, J. S. Pickett, and N. Cornilleau-Wehrlin (2006), Propagation of whistler mode chorus to low altitudes: Spacecraft observations of structured ELF hiss, *J. Geophys. Res.*, *111*, A10208, doi:10.1029/2005JA011462.

Santolík, O., D. A. Gurnett, J. S. Pickett, S. Grimald, P. M. E. Decreau, M. Parrot, N. Cornilleau-Wehrlin, F. El-Lemdani Mazouz, D. Schriver, and A. Fazakerley (2010a), Wave-particle interactions in the equatorial source region of whistler-mode emissions, *J. Geophys. Res.*, *115*, A00F16, doi:10.1029/2009JA015218.

Santolík, O., J. S. Pickett, D. A. Gurnett, J. D. Menietti, B. T. Tsurutani, and O. Verkhoglyadova (2010b), Survey of Poynting flux of whistler mode chorus in the outer zone, *J. Geophys. Res.*, *115*, A00F13, doi:10.1029/2009JA014925.

Schriver, D., et al. (2010), Generation of whistler mode emissions in the inner magnetosphere: An event study, *J. Geophys. Res.*, *115*, A00F17, doi:10.1029/2009JA014932.

Sigsbee, K., J. D. Menietti, O. Santolík, and J. B. Blake (2008), Polar PWI and CEPPAD observations of chorus emissions and radiation belt electrons: Four case studies, *J. Atmos. Sol. Terr. Phys.*, *70*, 1774–1788, doi:10.1016/j.jastp.2008.02.005.

Sigsbee, K., J. D. Menietti, O. Santolík, and J. S. Pickett (2010), Locations of chorus emissions observed by the Polar plasma wave instrument, *J. Geophys. Res.*, *115*, A00F12, doi:10.1029/2009JA014579.

Smith, E. J., and B. T. Tsurutani (1976), Magnetosheath lion roars, *J. Geophys. Res.*, *81*, 2261–2266, doi:10.1029/JA081i013p02261.

Sonnerup, B. U. Ö., and L. J. Cahill Jr. (1967), Magnetopause structure and attitude from Explorer 12 observations, *J. Geophys. Res.*, *72*, 171–183, doi:10.1029/JZ072i001p00171.

Storey, L. R. O. (1959), A method for measuring local electron density from an artificial satellite, *J. Res. Natl. Bur. Stand. U.S.*, *63D*, 325–340.

Summers, D., R. M. Thorne, and F. Xiao (1998), Relativistic theory of wave-particle resonant diffusion with application to electron acceleration in the magnetosphere, *J. Geophys. Res.*, *103*, 20,487–20,500, doi:10.1029/98JA01740.

Summers, D., C. Ma, N. P. Meredith, R. B. Horne, R. M. Thorne, and R. R. Anderson (2004), Modeling outer-zone relativistic electron response to

whistler mode chorus activity during substorms, *J. Atmos. Sol. Terr. Phys.*, *66*, 133–146, doi:10.1016/j.jastp.2003.09.013.

Summers, D., B. Ni, and N. P. Meredith (2007a), Timescales for radiation belt electron acceleration and loss due to resonant wave particle interactions: 1. Theory, *J. Geophys. Res.*, *112*, A04206, doi:10.1029/2006JA011801.

Summers, D., B. Ni, and N. P. Meredith (2007b), Timescales for radiation belt electron acceleration and loss due to resonant wave-particle interactions: 2. Evaluation for VLF chorus, ELF hiss, and electromagnetic ion cyclotron waves, *J. Geophys. Res.*, *112*, A04207, doi:10.1029/2006JA011993.

Thorne, R. M., T. P. O'Brien, Y. Y. Shprits, D. Summers, and R. B. Horne (2005), Timescale for MeV electron microburst loss during geomagnetic storms, *J. Geophys. Res.*, *110*, A09202, doi:10.1029/2004JA010882.

Torrence, C., and G. P. Compo (1998), A practical guide to wavelet analysis, *Bull. Am. Meteorol. Soc.*, *79*, 61–78, doi:10.1175/1520-0477(1998)079<0061:APGTWA>2.0.CO;2.

Tsurutani, B. T. (1972), Energetic electron precipitation and substorms, Ph.D. thesis, Dep. of Phys., Univ. of Calif., Berkeley.

Tsurutani, B. T., and W. D. Gonzalez (1987), The cause of high-intensity long-duration continuous *AE* activity (HILDCAAs): Interplanetary Alfvén wave trains, *Planet. Space Sci.*, *35*, 405–412, doi:10.1016/0032-0633(87)90097-3.

Tsurutani, B. T., and G. S. Lakhina (1997), Some basic concepts of wave particle interactions in collisionless plasmas, *Rev. Geophys.*, *35*, 491–501, doi:10.1029/97RG02200.

Tsurutani, B. T., and E. J. Smith (1974), Postmidnight chorus: A substorm phenomenon, *J. Geophys. Res.*, *79*, 118–127, doi:10.1029/JA079i001p00118.

Tsurutani, B. T., and E. J. Smith (1977), Two types of magnetospheric ELF chorus and their substorm dependences, *J. Geophys. Res.*, *82*, 5112–5128, doi:10.1029/JA082i032p05112.

Tsurutani, B. T., E. J. Smith, H. I. West Jr., and R. M. Buck (1979), Chorus, energetic electrons and magnetospheric substorms, in *Wave Instabilities in Space Plasmas*, edited by P. Palmadesso and K. Papadopoulos, pp. 55–62, D. Reidel, Dordrecht, Netherlands.

Tsurutani, B. T., W. D. Gonzalez, F. Tang, S.-I. Akasofu, and E. J. Smith (1988), Origin of interplanetary southward magnetic fields responsible for major magnetic storms near solar maximum (1978–1979), *J. Geophys. Res.*, *93*, 8519–8531, doi:10.1029/JA093iA08p08519.

Tsurutani, B. T., X.-Y. Zhou, V. M. Vasyliunas, G. Haerendel, J. K. Arballo, and G. S. Lakhina (2001), Interplanetary shocks, magnetopause boundary layers and dayside auroras: The importance of a very small magnetospheric region, *Surv. Geophys.*, *22*, 101–130, doi:10.1023/A:1012952414384.

Tsurutani, B. T., et al. (2006), Corotating solar wind streams and recurrent geomagnetic activity: A review, *J. Geophys. Res.*, *111*, A07S01, doi:10.1029/2005JA011273.

Tsurutani, B. T., O. P. Verkhoglyadova, G. S. Lakhina, and S. Yagitani (2009), Properties of dayside outer zone chorus during HILDCAA events: Loss of energetic electrons, *J. Geophys. Res.*, *114*, A03207, doi:10.1029/2008JA013353.

Tsyganenko, N. A. (1989), A magnetospheric magnetic field model with a warped tail current sheet, *Planet. Space Sci.*, *37*, 5–20, doi:10.1016/0032-0633(89)90066-4.

Tsyganenko, N. (2002), A model of the near magnetosphere with a dawn-dusk asymmetry: 1. Mathematical structure, *J. Geophys. Res.*, *107*(A8), 1179, doi:10.1029/2001JA000219.

Verkhoglyadova, O. P., and B. T. Tsurutani (2009), Polarization properties of Gendrin mode waves observed in the Earth's magnetosphere: Observations and theory, *Ann. Geophys.*, *27*, 4429–4433, doi:10.5194/angeo-27-4429-2009.

Verkhoglyadova, O. P., B. T. Tsurutani, Y. Omura, and S. Yagitani (2009), Properties of dayside nonlinear rising tone chorus emissions at large L observed by Geotail, *Earth Planets Space*, *61*, 625–628.

Verkhoglyadova, O. P., B. T. Tsurutani, and G. S. Lakhina (2010), Properties of obliquely propagating chorus, *J. Geophys. Res.*, *115*, A00F19, doi:10.1029/2009JA014809.

Zhou, X., and B. T. Tsurutani (1999), Rapid intensification and propagation of the dayside aurora: Large scale interplanetary pressure pulses (fast shocks), *Geophys. Res. Lett.*, *26*, 1097–1100, doi:10.1029/1999GL900173.

B. J. Falkowski, B. T. Tsurutani, and O. P. Verkhoglyadova, Jet Propulsion Laboratory, California Institute of Technology, Pasadena, CA 91109, USA. (bruce.tsurutani@jpl.nasa.gov)

G. S. Lakhina, Indian Institute of Geomagnetism, Navi Mumbai 410 218, India.

J. S. Pickett, Department of Physics and Astronomy, University of Iowa, Iowa City, IA 52242, USA.

O. Santolík, Institute of Atmospheric Physics, Prague 14131, Czech Republic.